Time Domain Acoustical Holography and Its Applications

Jørgen Hald, Brüel & Kjær Sound & Vibration Measurement A/S, Nærum, Denmark

This article describes Time Domain Acoustical Holography, its implementation in Brüel & Kjær's Non-Stationary Spatial Transformation of Sound Fields (NS-STSF) system and its application to solve a few noise source location problems in the automotive industry. Essentially, Time Domain Holography provides spatial mapping of a radiated sound field with a time resolution as short as the sampling interval of the A/D-converter used for the acquisition. The use of Envelope Intensity to view the time history of noise radiation is explained and verified. Three application examples are outlined. The first concerns localization of brake squeal noise sources. The second example deals with engine knocking noise (where and when noise is radiated as a function of crankshaft angle). In the third application, an engine run-up measurement is analyzed and selected engine orders are mapped to localize the origin of strong order-related noise components. A wealth of different analyses can be performed on a single fast time history recording taken with a microphone array and a tacho probe.

The principles of Brüel & Kjær's *Non-Stationary* STSF measurement system were developed and applied as a part of a sound field assessment task for the Brite-Euram research project PIANO which ended early in 1996. The PIANO project dealt with new methods to enable faster, cheaper and more accurate ISO 362 pass-by noise reduction measures for heavy road vehicles. This standard specifies a transient outdoor vehicle test and troubleshooting of components must be performed under similar conditions. Cross spectral based near-field acoustical holography implemented in Brüel & Kjær's STSF system[1,2] requires stationary signals and therefore did not apply.

Non-Stationary STSF (NS-STSF) is an implementation of Time Domain Holography (TDH).[3] TDH processes a recorded acoustic event that consists of simultaneously measured pressure time histories from a planar surface covering the sound source. As a consequence, nonsimultaneous data acquisition (scanning) cannot be used – a full-size microphone array is needed. Compared with STSF, the three most significant advantages of NS-STSF are:

1. Reference signals are not required.
2. There are no requirements for stationary operation of the sound source.
3. Full time resolution is retained throughout the NS-STSF measurement and the Time Domain Holography calculations.

Thus, while STSF provides detailed information about where noise is radiated, NS-STSF can show both where and when noise is radiated. While STSF takes into account only that part of the sound field which is coherent with the reference signals, NS-STSF operates with a full representation of the sound field.

This article briefly describes the principles and theory of NS-STSF, including the use of envelope intensity to overview the sometimes very complicated time variations encountered. Some typical application examples are given.

Principles of NS-STSF

Time Domain Holography maps all sound field descriptors (pressure, particle velocity, intensity, etc.) in the near field, not only as a function of physical location but also as a function of time. A TDH measurement can be seen as a sequence of snapshots of the instantaneous pressure over the array area, the time separation between subsequent snapshots being equal to the sampling interval in the A/D conversion. Similarly, the basic output of TDH is a time sequence of snapshots of a selected acoustical quantity in a calculation plane parallel with the measurement plane. An example is given in Figure 1, which contains a sequence of snapshots of instantaneous air particle displacement over a calculation plane at the sidewall of a truck tire.

When NS-STSF is applied to engine noise analysis, two crankshaft tacho signals are normally recorded simultaneously with the array signals – one high resolution tacho for precise measurement of the crank angle rotation and another once per cycle tacho for identification of a reference angular position. These two tacho signals allow the crank angle at the time of each snapshot to be identified in addition to engine RPM. With the NS-STSF system it is therefore possible to visualize radiation and, at the same time, relate it to different events during an engine cycle.

Figure 2 shows the NS-STSF data flow in schematic form. Notice that averaging is an option – it is possible to display measurements using sample rate time resolution. Sequences of maps can be animated as illustrated in Figure 1 to provide a visual understanding of the sound radiation process.

When no averaging is performed and the output is in the form of time signals, these signals can be exported to any type of post-processing. For example, exported pressure time signals can be used for subjective sound evaluation using the Brüel & Kjær PULSE Sound Quality software Type 7698.

Similar to the STSF software, the NS-STSF software can also simulate source modification by attenuating a particle velocity map over selected subareas of a plane at the source surface. The sound field of the modified source can then be calculated and investigated. For example, pressure time signals at some distance can be calculated and exported for subjective sound evaluation. The noise control engineer can thereby predict the sound after a simulated modification of the sound source. Possibly the most important practical benefit of the NS-STSF system is the ability to extract any information about the radiated sound from a single fast recording with a microphone array.

Instrumentation

The microphone array consists of a large number of specially designed low-cost Brüel & Kjær Array Microphones Type 4935 that can be clipped into position in an open grid network. Figure 3 shows an array with 10 columns and 12 rows of microphones fitted into the Integral Connection Array Type WA0806. The microphones do not need individual cabling. Instead, groups of six microphones are fitted into a tube with integrated cabling to a single LEMO connector. The six microphones are then connected to the transducer signal conditioner with a single cable.

The signal conditioner is a Brüel & Kjær Intelligent Data Acquisition (IDA) front end system Type 3561. Time history data are stored in real time in the signal conditioner. After the recording is completed, data are transferred through a standard Ethernet interface to the host computer running the Non-Stationary STSF software Type 7712. The IDA front end can handle up to 3000 channels in multiple frames.

The software includes dedicated functionality to facilitate the handling of the large number of measurement channels often required for the NS-STSF application. For example, a Detect function automates the definition of the array (row,

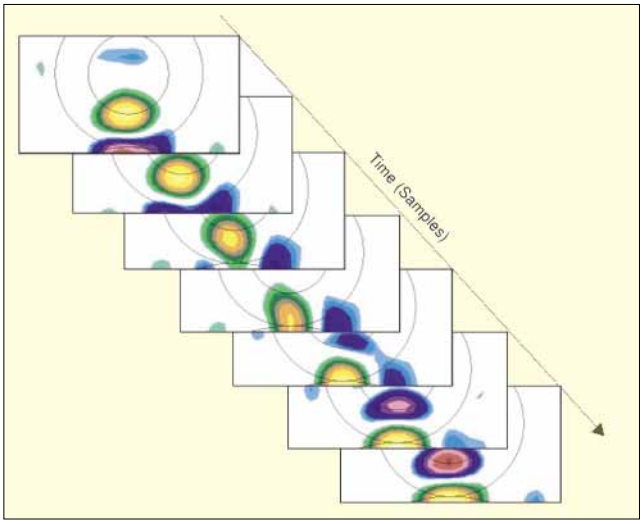

Figure 1. Illustration of combined space and time resolution. The maps represent instantaneous air particle displacement over a plane at the sidewall of a tire. Green/yellow colors represent outward deflection. Blue/red colors represent inward deflection.

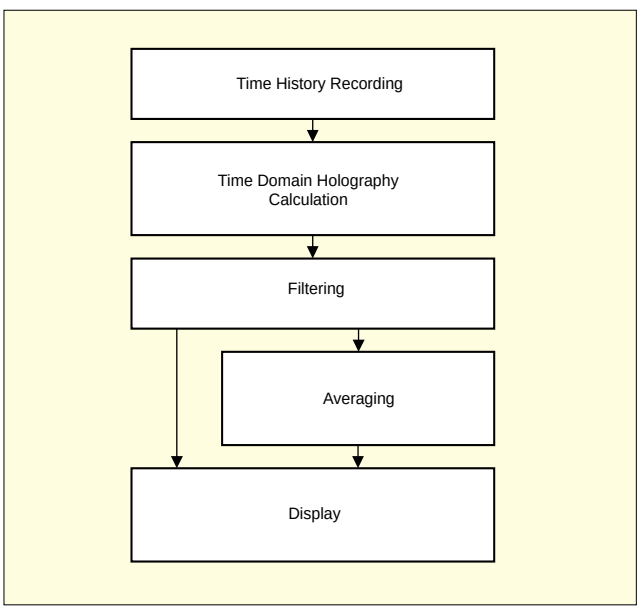

Figure 2. Data flow in NS-STSF.

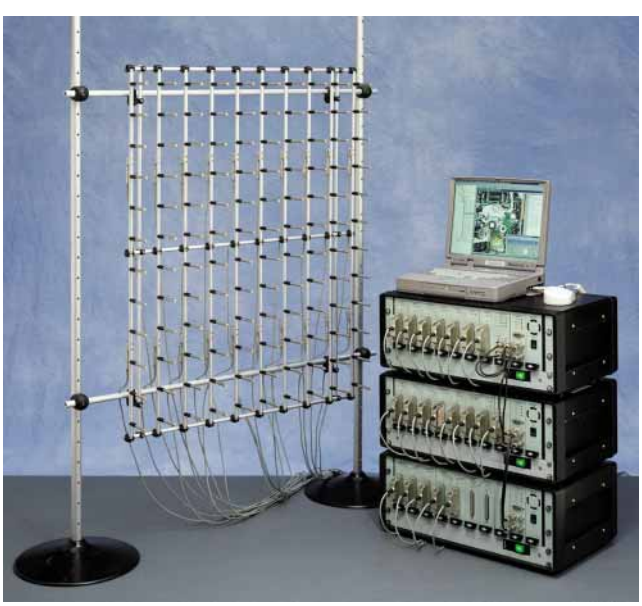

Figure 3. 120 element microphone array, IDA front-end and computer for NS-STSF.

Plane and Evanescent Waves

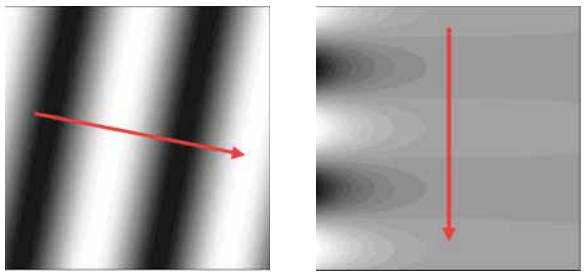

The two figures illustrate a plane wave and an evanescent wave, respectively. A red arrow indicates the direction of wave propagation. The "source plane" $z = -d$ constitutes the leftmost limitation in each figure, so the measurement plane is vertical a bit to the right of the source plane. White color represents the highest positive instantaneous pressure, black represents the largest negative instantaneous pressure and a gray color in the middle represents zero instantaneous pressure. The temporal angular frequency ω is the same in both figures, and for the plane wave the distance along the propagation direction between two neighboring pressure maxima is equal to the wavelength (or period length) λ. The spatial angular frequency of the plane wave along its direction of propagation is therefore

$$k = \frac{2\pi}{\lambda} = \frac{\omega}{c}$$

where c is the propagation speed of sound. Notice that the spatial variation of the plane wave in the xy-plane is always slower than the variation along the propagation direction. In mathematical terms, the spatial angular frequency vector (k_x,k_y) of a plane wave in the xy-plane is always shorter than the spatial angular frequency k along the propagation direction:

$$k_x^2 + k_y^2 \le k^2 \quad \text{(plane wave)}$$

Higher spatial frequencies in the xy-plane therefore cannot represent plane waves. They represent so-called Evanescent waves. The right figure shows an example with $k_x^2 + k_y^2 = (1.1k)^2$. In any xy-plane the evanescent wave looks exactly like a plane wave, but in the z-direction it exhibits an exponential decay. The decay becomes faster with increasing spatial frequency.

column) connections to the front end channels (frame, module and channel). Calibration can be performed on six microphones in parallel using a special pistonphone adaptor and the system automatically detects which channels are being calibrated. Finally, there is extensive on-line monitoring of channel status, reporting for example: cable break; CCLD fault; and overload.

Time Domain Holography

Figure 4 illustrates the geometry of the measurement problem. The sound pressure $p(\mathbf{r},t) = p(x,y,z,t)$ is measured over the plane $z = 0$ in the near field region of a sound source. All parts of the source are assumed to be in the half space $z < -d$, d being the smallest distance between the source and the measurement plane. The half space $z \ge -d$ is assumed to be source-free and homogeneous.

The basic task performed by Time Domain Holography is to calculate the pressure $p(\mathbf{r},t)$ in a plane $z = constant \ne 0$ parallel with the measurement plane. It is shown in the Appendix that this calculation can be performed through a Fourier transform in the three dimensions (x,y,t). The output of the Fourier

transform is a representation of the pressure data in a spatial and temporal angular frequency domain (k_x,k_y,ω). Here, k_x and k_y are spatial angular frequencies (wave numbers) in the x- and y-directions, respectively. It is also shown in the Appendix, that, in this three dimensional frequency domain, the pressure is actually represented as an infinite sum of plane propagating waves (low spatial frequencies) and evanescent waves (high spatial frequencies). The evanescent waves die out exponentially in the z-direction away from the source. If we sum up (superimpose) all these elementary waves in the calculation plane, we obtain the pressure in that plane. This summation has the form of an inverse Fourier transform in the three dimensions (k_x,k_y,ω).

Figure 5 illustrates the Time Domain Holography calculation scheme, starting with the pressure in the measurement plane $z = 0$ and ending up with the pressure in the calculation plane $z = constant \neq 0$. According to the scheme, the transition from the measurement plane to the calculation plane is performed through multiplication with a transfer function H in the three dimensional frequency domain (k_x,k_y,ω). It is shown in the Appendix – see Equations (A5) and (A6) – that this transfer function has the following form:

$$H = e^{-jk_z z} \quad , z \geq -d \tag{1}$$

where the new spatial angular frequency k_z in the z-direction is a function of the angular frequencies (k_x,k_y,ω) associated with the measured data:

$$k_z \equiv \begin{cases} \sqrt{k^2 - k_x^2 - k_y^2} & \text{for } k_x^2 + k_y^2 \leq k^2 \quad \text{(plane waves)} \\ -j\sqrt{k_x^2 + k_y^2 - k^2} & \text{for } k_x^2 + k_y^2 > k^2 \quad \text{(evanescent waves)} \end{cases} \qquad k \equiv \frac{\omega}{c} \tag{2}$$

Here, $k \equiv \omega/c$ is the wave number. Clearly, the plane wave components undergo just a phase shift between the two planes, while the evanescent wave components are exponentially attenuated in the direction away from the source.

In order to estimate the particle velocity vector $\mathbf{u}(\mathbf{r},t)$ in the calculation plane, one just has to replace the transfer function H with a transfer function $\mathbf{H}_u$ that provides the particle velocity vector of each of the elementary waves (plane and evanescent) in the calculation plane. According to the Appendix, this transfer function has the following form:

$$\mathbf{H}_u = (\rho c)^{-1} \hat{\mathbf{k}} e^{-jk_z z} \tag{3}$$

where $\hat{\mathbf{k}} \equiv \mathbf{k}/k$ is a normalized form of the wave number vector $\mathbf{k} \equiv \{k_x, k_y, k_z\}^T$, c is the propagation speed of sound and ρ is the density of the homogeneous medium. For the plane wave components, $\hat{\mathbf{k}}$ is a unit vector in the propagation direction of the plane wave.

Having calculated the pressure $p(\mathbf{r},t)$ and the particle velocity vector $\mathbf{u}(\mathbf{r},t)$ time histories in the plane $z = constant \neq 0$, any type of filter (e.g., a frequency band filter or an order tracking filter) can be applied to the signals, and the instantaneous intensity vector $\mathbf{I}(\mathbf{r},t)$ can be obtained as the product of the two quantities:

$$\mathbf{I}(\mathbf{r},t) = p(\mathbf{r},t)\,\mathbf{u}(\mathbf{r},t) \tag{4}$$

Finally, averaging in time, RPM, shaft angle or engine cycle intervals can be performed on the calculated time signals.

Practical Implementation Considerations. So far we have assumed the pressure to be known continuously over an infinite plane and over an infinite time record. In practice we can, of course, only measure and represent discrete signals over finite windows in the three dimensions (x,y,t). If the signals are band limited in the three dimensions, then there is no loss of information when replacing the continuous signals with sampled versions, provided the sampling intervals are sufficiently small. From Equations (1) and (2) it follows that the high spatial frequencies are exponentially attenuated in the direction away from the source and in such a way that at any non-zero distance the pressure distribution will be, in practice, spatially band limited. In the time dimension we can make the

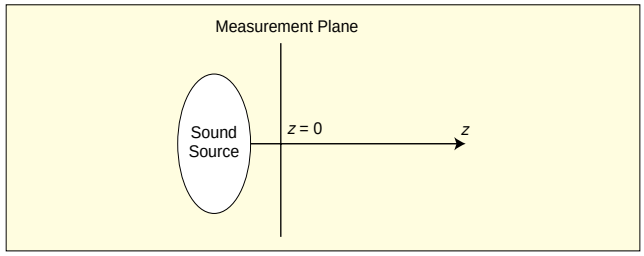

Figure 4. Measurement geometry.

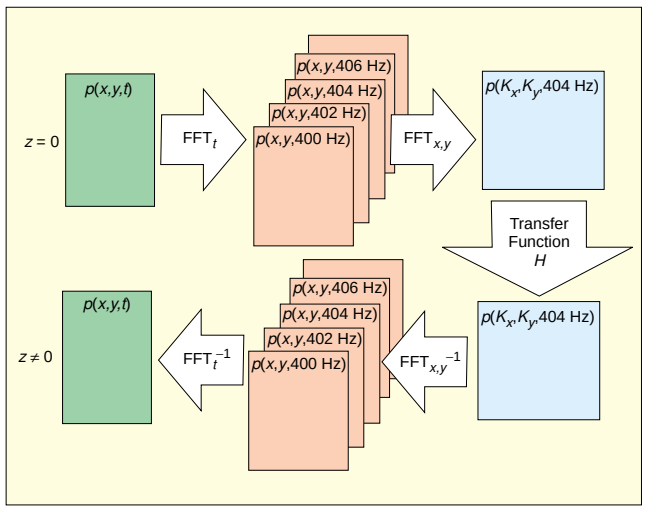

Figure 5. Data flow chart for time domain holography.

signals band limited through the use of anti-aliasing filters. The limited window size is more of a problem because information is lost and because it leads to spectral leakage in connection with the Fourier transform.

Various techniques exist to reduce the spatial windowing effects. The one that is usually most efficient and therefore applied in NS-STSF is the so-called *Velocity Windowing* technique, which is described in Reference 4. In this, a distribution of z-oriented particle velocity is initially calculated in a *Source Plane* which is parallel to the measurement plane and which is also close to the real source surface. All other sound field calculations are then based on that so-called *Surface Velocity* map. The Surface Velocity map covers an area with the same size as the array, so the obvious question might be, why the finite size of the Surface Velocity map does not lead to spatial windowing effects, just like the finite area of the pressure distribution measured by the array. The answer is that it does lead to spatial windowing errors but usually much less than the pressure window in the measurement plane. This is because the particle velocity vector in the Source Plane will have a very small z-component outside the area of the Surface Velocity map – here the vector will tend to be parallel with the source plane. From the z-component of the particle velocity we can calculate all other components of the sound field according to Rayleigh's first integral formula.[1]

In a practical implementation, the three dimensional Fourier transforms in (x,y,t) are calculated using the Discrete Fourier Transform (DFT). After the DFT transformation to the temporal and spatial frequency domains, the sound field is represented by a discrete three dimensional data set in these frequency domains. Such a discrete data set represents a signal which is periodic in both the time domain and in the spatial domain. When we calculate the sound field in a plane parallel with the measurement plane, the periodic spatial replica of the true measurement aperture will contribute over the entire calculation plane – also inside the area corresponding to the measurement aperture. Since the major part of this error comes from the nearest part of the first replica and since this part is just the opposite end of the measurement aperture itself, the sound field seems to "wrap around." The method

used to suppress this *Wrap Around Error* is to push the replica further away by zero padding the measured data before the DFT. A similar wrap around error will also be introduced in the time dimension and as in the spatial dimensions it is suppressed by zero padding.

The temporal window needs special attention in the NS-STSF application. In usual Fast Fourier Transform (FFT) based frequency analysis, a smooth temporal window – such as a Hanning window – is used to minimize the spectral leakage, without sacrificing too much spectral resolution. The focus is entirely on spectral estimation. In NS-STSF it is still important to get rather good spectral estimation because the spatial transformations involve the use of strongly frequency dependent transfer functions, such as in Equation (1). However, after multiplication with transfer functions in the frequency domain, the data need to be transformed back to the temporal domain by the use of the inverse FFT. If, for example, a Hanning window had been used before the forward FFT, then after the inverse FFT, the Hanning window would still be in effect. In order to remove this window function from the output time signals, one might attempt to divide by the same Hanning window. Close to the ends of the signals this would, however, mean division by a number close to zero. If no processing had been performed in the frequency domain, this would cause problems only in a very narrow interval at the two ends of the signals. But, the processing performed in the frequency domain will include delays, because wave propagation takes time. Signal components delayed to an end interval of the time record will be divided by a number close to zero and therefore be amplified far too much. A good solution has been found to be a Gaussian window given by the expression:

$$w_i = e^{-(1/2)\left(a\frac{2i-N}{N}\right)^2}, \quad i = 0, 1, \ldots (N-1), \; a = 2.6 \qquad (5)$$

where N is the number of samples in the time record.[5] The window function and its normalized FFT spectrum are shown in Figures 6 and 7, respectively. Because the window function does not approach zero towards the ends of the record, we can divide the output time signals by the window function without getting the problem of dividing by very small numbers. Further, the Gaussian window provides a very good combination of low spectral leakage (low side-lobe level in the window spectrum) and high spectral resolution (narrow main lobe in the window spectrum).

An example illustrates the use of FFT processing in NS-STSF. Consider a measurement by an array with 12 rows and 10 columns and assume a 2 sec recording with 8K samples/sec sampling rate. Thus, we have 120 simultaneously measured time records, each with a length equal to 16K samples. The zero-padding in the *x*- and *y*-dimensions will typically result in an extended data grid with 32 rows and 32 columns, so the FFTs in these dimensions will be operating with data records of length equal to 32 samples. Neglecting the zero padding in time, the FFT in the time dimension must be performed on one long record of length 16K samples because the FFT should approximate the continuous Fourier transform.

Envelope Active and Reactive Intensity

Having described important aspects of the holography calculations, we now turn to post-processing. The Instantaneous Intensity $\mathbf{I}(\mathbf{r},t)$ consists of a reactive part, representing spatially oscillating energy that does not carry any average acoustical energy flow, and an active part which oscillates around a time varying local average. This time varying average is called the envelope active intensity; while the time varying amplitude of the reactive component is called the envelope reactive intensity. The active part of the instantaneous intensity oscillates from zero to a time varying peak value around the envelope active intensity. Figure 8 shows (in black) the oscillating instantaneous intensity for a measurement of broadband noise filtered to a 1/3-octave frequency band and on top of that curve, the envelope active intensity is seen (in red) as a time varying

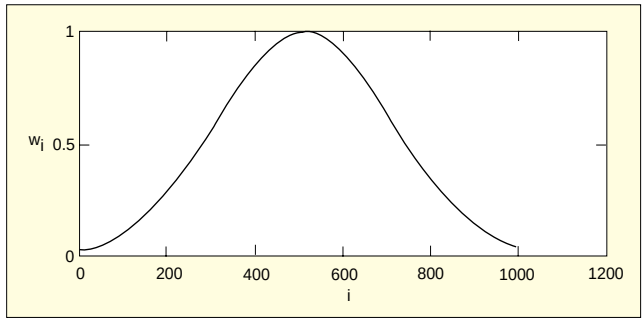

Figure 6. Gaussian window function, shown for an N =1024 sample record.

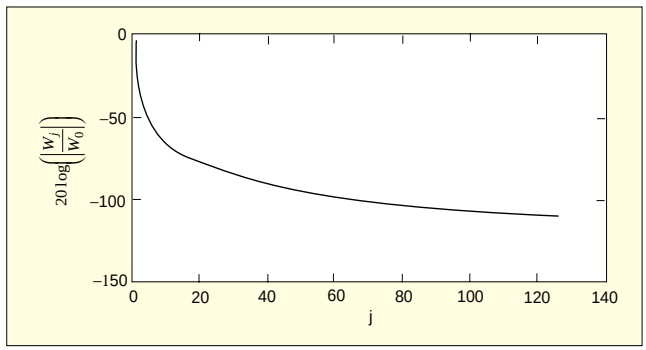

Figure 7. Normalized spectrum of the Gaussian window function in Figure 6, showing only the first 128 frequency lines.

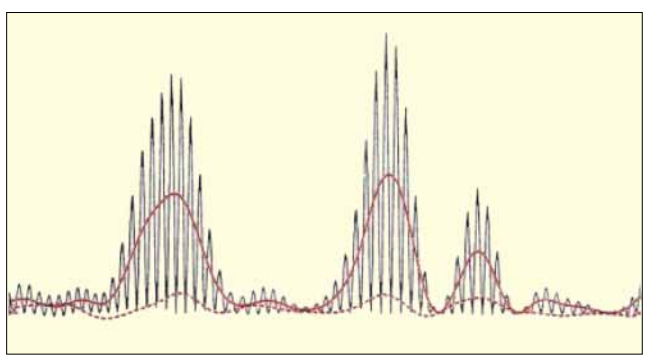

Figure 8. Instantaneous Intensity (black), envelope active intensity (red) and envelope reactive intensity (red, dashed).

local average.[6] The dashed red curve represents the envelope reactive intensity. Clearly, the active component is much stronger than the reactive component in this example.

Animation of a time sequence of maps of the instantaneous intensity $\mathbf{I}(\mathbf{r},t)$ will provide, in many cases, an overwhelming amount of information. Since both the active and the reactive parts are strongly oscillating, one will often see a very complicated picture with fluctuating peaks of positive and negative instantaneous intensity. And, it will be difficult to view, where the active component is strong and where predominantly reactive intensity is seen. The solution adopted in NS-STSF is to look at the slowly time varying envelope active (and reactive) intensity.

The envelope active intensity $\bar{\mathbf{I}}(\mathbf{r},t)$ is obtained through calculation of the signals $\hat{p}(\mathbf{r},t)$ and $\hat{\mathbf{u}}(\mathbf{r},t)$, which are Hilbert transforms in time of the pressure $p(\mathbf{r},t)$ and the particle velocity vector $\mathbf{u}(\mathbf{r},t)$, respectively, see Reference 7 for a description. In Reference 7 it is shown that for finite energy signals – to which group most transient signals belong – the envelope active intensity signal $\bar{\mathbf{I}}(\mathbf{r},t)$ represents the same total energy per unit area over time as the instantaneous intensity signal $\mathbf{I}(\mathbf{r},t)$.

Measurements

The following two sections present two NS-STSF applications which clearly distinguish the technique from scan based acoustical holography implementations, such as the STSF sys-

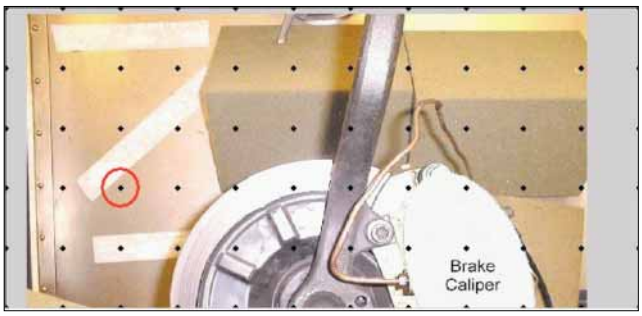

Figure 9. Measurement area with indication of array microphone positions (dots).

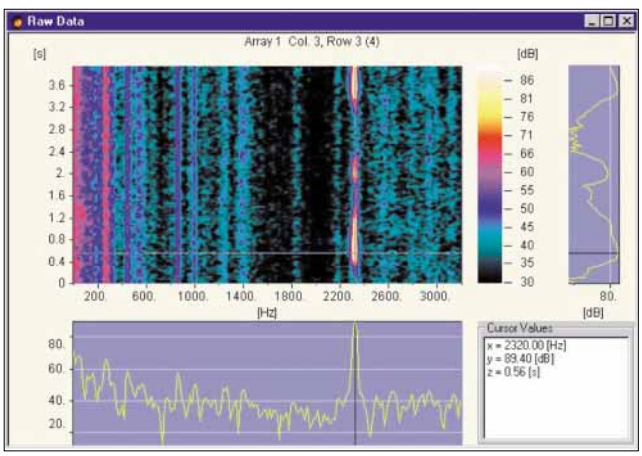

Figure 10. Time/frequency plot in Brüel & Kjær NS-STSF Type 7712 raw data view (looking only at measured signals – not calculated data). A time slice at 2320 Hz and a frequency spectrum at 0.56 sec are selected by the contour cursor and displayed at the right hand side and at the bottom, respectively.

tem.

Capturing and Mapping a Transient Acoustical Event. The first example that we shall consider is measurement of disk brake squeal. Since squeal noise is transient by nature and very difficult to reproduce in a controlled way, a scanning holography method is not suitable. With NS-STSF, only a single recording is sufficient to get detailed temporal and spatial information about the squeal noise radiation.

Figure 9 shows a picture of the part of the brake disk over which the measurement was taken. The microphone positions are indicated by dots. Because of the supporting structure it was not possible to measure the entire area of the disk. As seen in the illustration, an array with 6 rows and 12 columns was used to measure the upper half of the inside of the disk. The array element spacing was 5 cm, covering a frequency range up to approximately 3 kHz, and the distance from the disk to the array was approximately 10 cm. A 4 sec recording with 3.2 kHz bandwidth was made.

Clearly, the array area did not cover the entire source as normally required. The part of the source outside the array area was shielded by absorbing material in order to approximately meet the requirement. Further, by use of the Velocity Windowing technique and by the use of a smaller *Dynamic Range* than normally applied in the reconstruction of evanescent waves, quite good results could be obtained anyway.

To inspect the temporal characteristics of the recorded squeal(s), the time history of selected microphone signals was plotted. In Figure 10 we have chosen the signal from the array microphone at column 3 and row 3, which is circled in Figure 9. Clearly, the signal is dominated by a narrow-band squeal component around 2320 Hz, and the 4 sec recording period is seen to contain actually three separate short squeals.

In order to calculate the sound field in some plane parallel with the array plane a calculation setup must be defined, see Figure 11. The primary parameters of that setup are:

- The time and frequency interval to be processed.

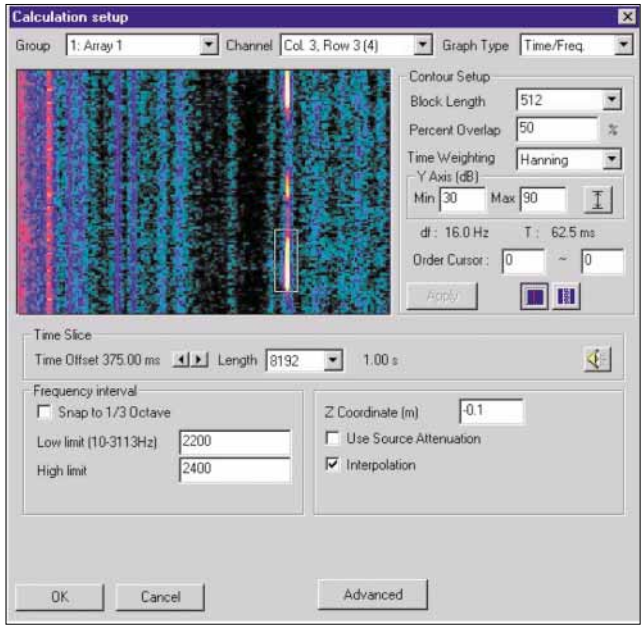

Figure 11. Calculation setup.

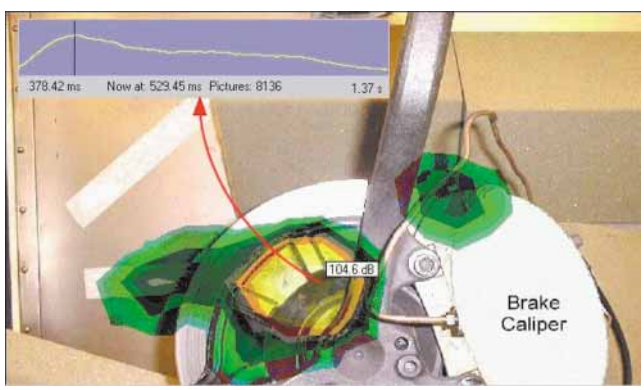

Figure 12. Contour plot of envelope active intensity. A time slice representing the position of the contour cursor is included. The contour interval is 1 dB.

- The Z-coordinate of the calculation plane.

The selection of time and frequency intervals can be based on the time/frequency plot for a selected microphone signal. Here, the same array microphone as used in the raw data view in Figure 10 has been chosen and the time/frequency interval selected for calculation is shown as a frame on top of the contour plot. The interval is seen to cover the time and frequency intervals of the first squeal. The calculation plane has been chosen to be close to the disk.

Figure 12 shows a contour plot of the envelope active intensity at the point in time where the peak value is highest. At the point in space where the peak occurs, the time slice of the envelope active intensity is shown in the top left corner. The time variation is seen to be very slow over the 1 sec interval of the calculated time record. This is because the frequency bandwidth of the signal is so narrow. Surprisingly, the area of highest radiation is not over the disk itself but over a less rigid cover plate.

Analyzing Micro Phenomena and Orders in Engine Noise Radiation. Two series of measurements were taken over the front and the left side of a Daimler-Chrysler 2.3 liter engine, see Figure 13. For all measurements a sampling frequency equal to 8K samples/sec was used, supporting a frequency range up to 3.2 kHz. Each series included the following two recordings:

1. Stationary 4000 RPM, Full Load, 2 sec.
2. Run-up 1000-5400 RPM, Full Load, 10 sec.

The main purpose of the stationary measurements was to study the sound intensity map as a function of crankshaft angle.

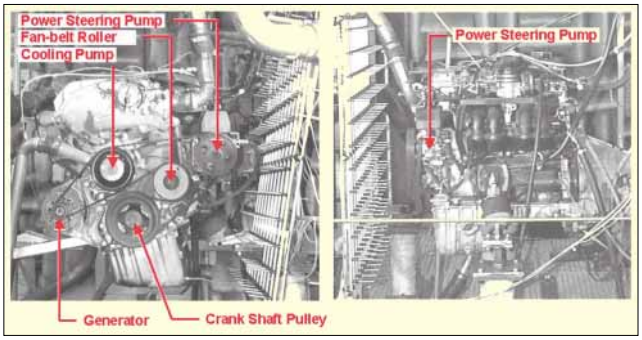

Figure 13. Front and left side pictures of the engine, also showing the microphone array.

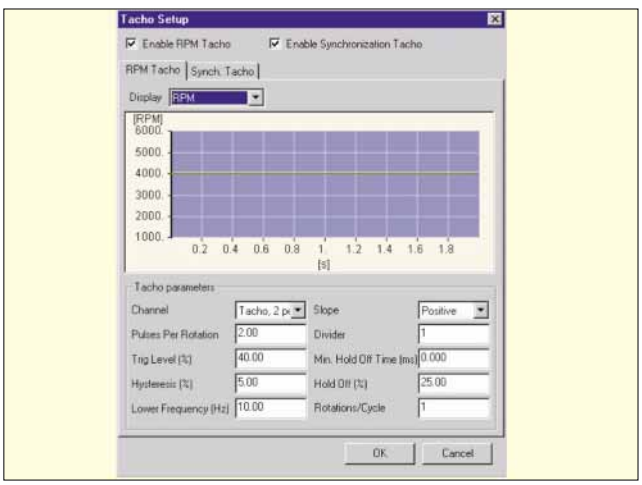

Figure 14. Tacho setup.

Figure 15. Average sound intensity at the engine surface for the 1 kHz 1/3-octave band. The contour interval is 1 dB.

This type of analysis can be used to gain understanding of the mechanism of knocking noise radiation. The objective of the run-up measurements was to display the intensity map of the dominating orders at different RPM values during run-up. This is useful in identifying the cause of annoying order components in the noise spectrum.

The measurements were taken with a 12×10 grid of Array Microphones Type 4935, i.e., there were 12 rows and 10 columns. With 7.5 cm grid spacing, the supported frequency range extends up to a bit above 2 kHz. The array size of 75 cm by 90 cm was sufficient to cover the major parts of the engine. Two tacho signals were recorded together with the array signals:

1. One pulse per two rotations for definition of crank angle equal to zero.
2. Two pulses per rotation for higher resolution angle definition.

First we shall look at the stationary 4000 RPM measurement over the engine front, with the purpose of studying the sound power radiation as a function of crankshaft angle. Figure 14 shows the tacho setup window, where the signals to be used for RPM and crank angle detection are selected and also the parameters for the detection are defined. The graphics area of the window can display time signal, detected tacho sequence and RPM graph. In this case the RPM graph has been selected.

During the analysis of the measured data for the engine front, it was discovered that the microphone in row 12 and column 9 (i.e., almost in the upper right corner) had a bad connection. The measured signal was just impulsive noise. Fortunately, we could use a so-called Bad Measurement Interpolation function of the NS-STSF software to disregard the bad signal and replace it by interpolated data, see Reference 7 for details.

We applied a 1/3 octave filter at 1 kHz, calculated the sound intensity over a plane at the surface of the engine and averaged over 1 sec. As a result we got a map of the average active intensity at the engine surface as shown in Figure 15. The areas of highest radiation are seen to be just below the crankshaft pulley and around the upper part of the fan belt roller.

In Figure 15 we have, of course, lost all time or crank angle resolution because of averaging. In order to obtain time or crank angle resolution, we skipped the averaging and calculated instead the envelope active intensity in the same plane at the engine surface. We still looked at the 1 kHz 1/3 octave band of the stationary 4000 RPM measurement.

Figure 16 shows four snapshots from left to right with a crank angle interval of 56°. The crank angle is shown in the top left corner of each plot. A position cursor can be seen at the lower limitation of the crankshaft pulley and the so called “properties window” below the sequence relates to that cursor position on the first plot in the sequence. The signal in the upper part of the properties window is the (envelope active intensity) time signal at the position cursor. Clearly, the signal at that position is very impulsive, indicating that a knocking type of sound might be radiated.

A time cursor is seen in one of the impulses, indicating the instant in time represented by the contour plot. Looking again at the plot sequence, we observe that the impulse below the crankshaft pulley precedes the sound radiation from the area over and around the fan belt roller (see Figure 13). The impulse below the crankshaft pulley is due to the firing of the front cylinder. The cylinder pressure is transmitted through the crankshaft into the engine block where noise is radiated. Subsequently, the deflection propagates to other parts of the engine. The high radiation around the fan belt roller could be due to transmission through the timing belt.

During animation, the properties window also shows the instantaneous RPM and corresponding crank angle. The crank angle indicators at the four instants in time represented in the plot sequence in Figure 16 have been copied onto the four plots.

With the NS-STSF software it is very easy to search the time/position data and to perform time animations: by clicking on a point in time, the contour plot at that time will be displayed; by clicking at a position in the contour plot, the time data for that position will be shown in the properties window. Animation is controlled by a standard set of playback controls. Several animations can be synchronized and run in parallel.

In Figure 16, the time slice showed a certain but not perfect periodicity of the intensity from cycle to cycle. If the aim is to obtain a good overview of the average radiation as a function of crank angle, then the time animation provides too much detail without giving the average picture.

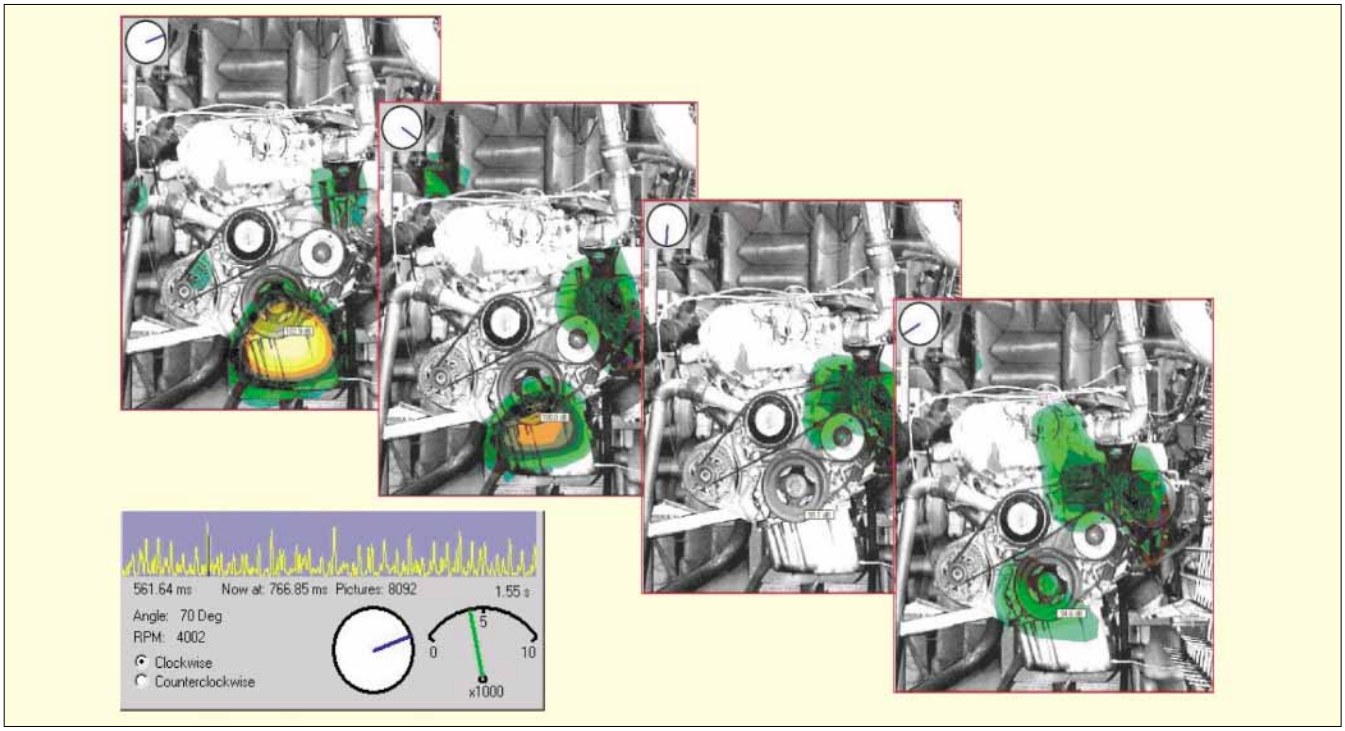

Figure 16. Envelope active intensity at four different crankshaft angles and, below, the time slice at the contour cursor position. Contour interval is 1 dB.

To provide this overview, the NS-STSF software can perform averaging into a set of angle intervals of specified equal width. For the engine front measurement we have chosen a 10° angular averaging interval width, leading to a set of 72 intervals over the 720° crankshaft rotation within a complete engine cycle.

In Figure 17 we again look at the active intensity in the 1 kHz 1/3 octave band, but averaged in 10° intervals. The two contour plots are identical, representing both the crank angle interval centered at 50° – only the cursor positions and the associated angle interval slices at the bottom are different. To the left, the contour cursor is over the oil sump and the angle slice for that position shows that we are at the crank angle where the intensity over the oil sump is at its maximum. To the right, the contour cursor is above the fan belt roller but we still look at the crank angle interval where the oil sump radiation peaks. The angle slice for the position above the fan belt roller shows that the radiation at that position peaks a bit later than the radiation from the oil sump. Another difference is that the oil sump radiation is rather concentrated in angle, whereas the radiation around the fan belt roller covers a rather broad crank angle interval. This example illustrates the possibility of quickly reading the radiation versus crank angle at many positions by clicking the contour cursor at these positions, looking at the angle slice in the properties window.

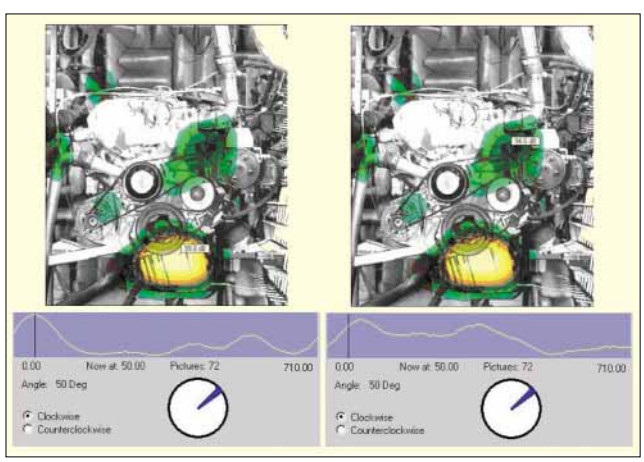

Figure 17. 1 kHz active intensity averaged over a 10° crank angle interval 50° after the firing of the front cylinder. The crank angle slices corresponding to the two contour cursor positions are seen at the bottom. Contour interval is 1 dB.

Figure 18 presents the same comparison of crank angle 'timing' of two hot spots of impulsive radiation just for the 1.6 kHz instead of the 1 kHz 1/3 octave band. Again, we have used averaging in 10° crank angle intervals but now we look at the angle interval at 180°, i.e., approximately half a crankshaft rotation after the firing of the front cylinder.

In the figure to the left (see Figure 18), the contour cursor is over the valve cover and the angle slice at the bottom shows that we are looking at the angle where the radiation from the valve cover peaks. Notice that most of the radiation is concentrated within a rather small angular interval. To the right we look at the same map (i.e., for the same crank angle) only the contour cursor is now over the oil sump. The angle slice for the radiation from the oil sump shows a peak before the angle cursor, i.e., before the peak radiation over the valve cover. So, apparently the impulsive radiation from the oil sump precedes the impulsive radiation from the valve cover.

We next turn to the run-up measurements from 1000 to 5400

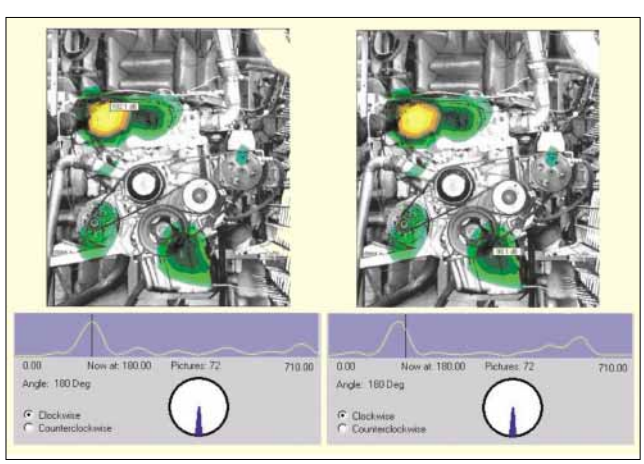

Figure 18. 1.6 kHz active intensity averaged over a 10° crank angle interval 180° after the firing of the front cylinder. The crank angle slices corresponding to the two contour cursor positions are seen at the bottom. Contour interval is 1 dB.

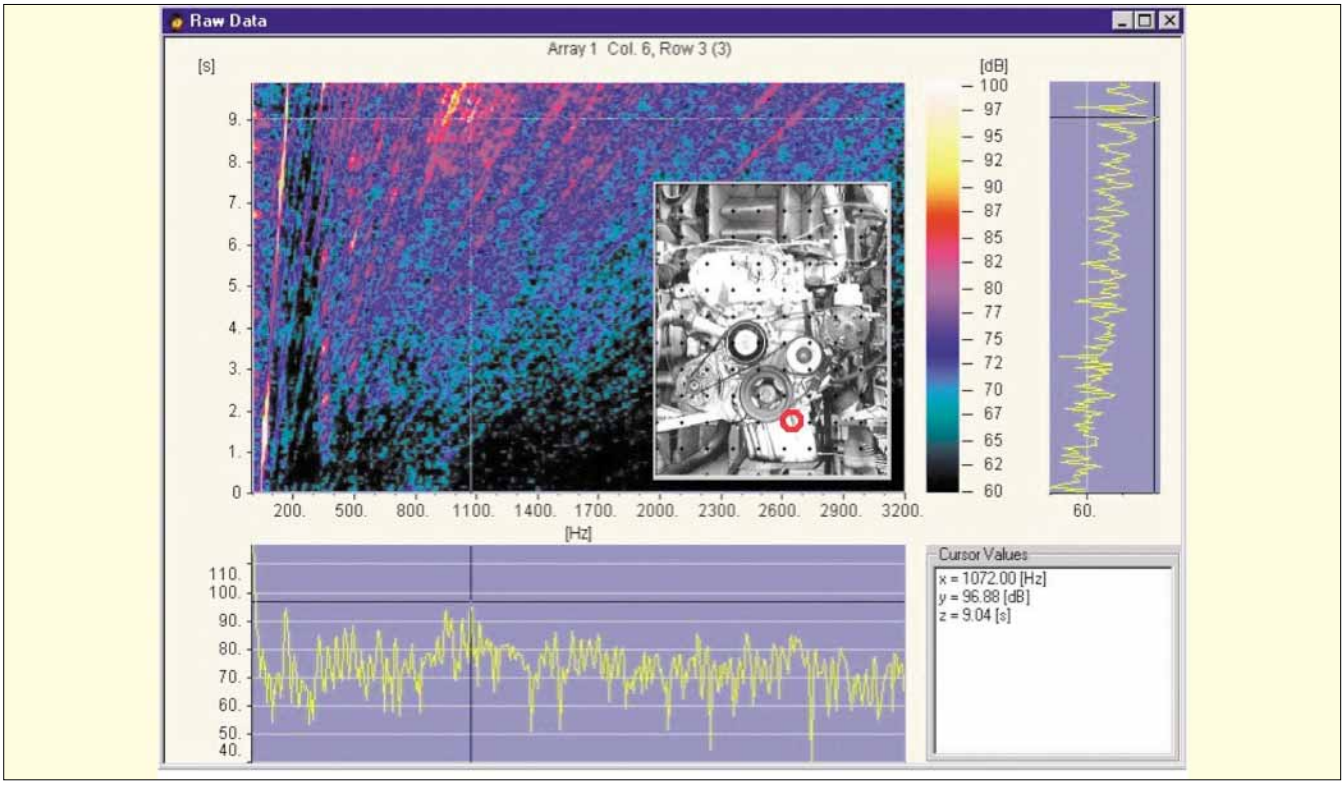

Figure 19. Time against frequency plot of the signal from a microphone placed alongside the oil sump (red circle). A time slice at 1072 Hz and a frequency spectrum at 9.04 sec are selected by the contour cursor and displayed at the right hand side and at the bottom, respectively.

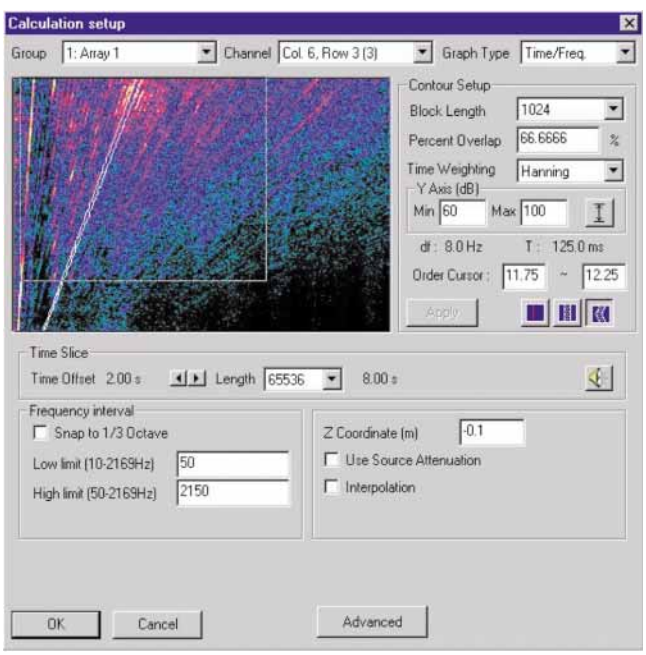

Figure 20. Calculation setup used with run-up test.

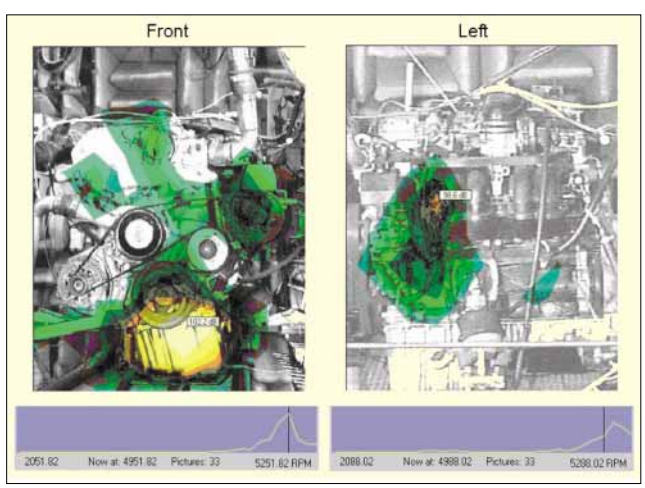

Figure 21. Active intensity of 13th engine order at the front and at the left side of the engine. The intensity is averaged over an interval of width 100 RPM around 4950 RPM. Contour interval is 1 dB.

RPM (full load on the engine) and we shall start with the measurement over the engine front. A time/frequency plot of the signal from an array microphone alongside the oil sump shows a very high level of the 13th order about 1 sec before the end of the 10 sec recording (see Figure 19). We will focus our attention on the 13th order.

Figure 20 shows the calculation setup, where the time and frequency intervals for the processing have to be selected. To facilitate this selection, we look at the same time against frequency plot as in Figure 19, but now the order interval between the 12.75th and the 13.25th order is shown on top of the plot. The rectangle represents the time and frequency intervals chosen for calculation – clearly the order band falls within the calculation window which covers the run-up from 2000 to 5400 RPM. Again the calculation plane is chosen to be at the engine surface.

In the display setup we select the order filter extracting the order interval from 12.75 to 13.25, and we select averaging of sound intensity in RPM intervals of 100 RPM width. As a result of the holography calculation and the averaging, we obtain a sequence of contour plots of active intensity covering the set of RPM intervals of 100 RPM width from 2000 to 5400 RPM. This has been done for both the front measurement and for the measurement on the left side.

Figure 21 shows the intensity maps on the front and left for the RPM interval around 4950 RPM. For each of the two contour plots, the RPM slice at the cursor position is shown below the plot.

The dominating peak on the front is seen to be over the oil sump, so we have positioned the contour cursor in that position. From the RPM slice under the contour plot we then see

that we are looking at the RPM interval where the intensity level at the contour cursor position has a sharp maximum. Looking at the contour plot, a smaller peak is seen between the power steering pump and the engine block.

The dominating peak on the left side of the engine (see Figure 21) is between the power steering pump and the air intake manifold. From the RPM slice at that position it can be observed that the level here is actually higher in the subsequent RPM interval, i.e., around 5050 RPM.

Conclusions

Using the NS-STSF system, the sound intensity, power, pressure, velocity and displacement maps from non-stationary noise sources can be obtained as a function of time, RPM, shaft angle or engine cycle in selected frequency or order bands. There is absolutely no restriction on the stationarity of the sound source – it can be anything from completely stationary to highly transient like a door slam.

All types of output data are available as time signals (with A/D converter sample rate) or averaged in time, RPM, shaft angle or engine cycle intervals of user specified width. Looking for the hot spots in time and space of transient sound energy radiation, an overview is conveniently obtained by looking at a time varying envelope active intensity map. All this information is available after a single very fast time history recording with a simple microphone array.

Acknowledgments

Bosch is acknowledged for allowing me to use the brake squeal measurement and DaimlerChrysler is acknowledged for letting me use the engine measurements.

References

1. Maynard, J. D., Williams, E. G. & Lee, Y., "Nearfield Acoustic Holography: I. Theory of Generalized Holography and the Development of NAH," *J. Acoust. Soc. Am.*, 78 (4), 1985, pp 1395-1413.
2. Hald, J., "STSF – A Unique Technique for Scan-Based Near-field Acoustic Holography Without Restrictions on Coherence," *Brüel & Kjær Technical Review,* No. 1, 1989, pp 1-50.
3. Saemann, E. -U. & Hald, J., "Transient Tyre Noise Measurements Using Time Domain Holography," 1997, Proc. SAE.
4. Hald, J., "Reduction of Spatial Windowing Effects in Acoustical Holography," 1994, Proceedings Inter-Noise.
5. Harris, F. J., "On the Use of Windows for Harmonic Analysis With the Discrete Fourier Transform," Proc. IEEE, Vol. 66, No. 1, 1978, pp 51-83.
6. Jacobsen, F., "A Note on Instantaneous and Time-Averaged Active and Reactive Intensity," *J. Sound Vib.*, 147, 1991, pp 489-496.
7. Hald, J., "Non-stationary STSF," *Brüel & Kjær Technical Review*, No. 1, 2000, pp 1-36.

The author can be contacted at: jhald@bksv.com.

Theory of Time Domain Holography

Figure 4 illustrates the geometry of the measurement problem. The sound pressure is measured over a plane $z = 0$ in the near field region of a sound source. All parts of the source are assumed to be in the half space $z < -d$, d being the smallest distance between the source and the measurement plane. The half space $z \geq -d$ is assumed to be source-free and homogeneous.

The time domain sound pressure field $p(\mathbf{r},t)$ fulfills the homogeneous wave equation in the half space $z \geq -d$:

$$\nabla^2 p - \frac{1}{c^2}\frac{\partial^2 p}{\partial t^2} = 0, \quad z \geq -d \tag{A1}$$

c being the propagation speed of sound.

For any given z-coordinate, we now introduce the following Fourier transform pair of sound pressure in three dimensions (x,y,t):

$$p(x,y,z,t) = \frac{1}{(2\pi)^3}\int_{-\infty}^{\infty}\int_{-\infty}^{\infty}\int_{-\infty}^{\infty} P(k_x,k_y,z,\omega)\, e^{-j(k_x x + k_y y - \omega t)} dk_x\, dk_y\, d\omega \tag{A2}$$

$$P(k_x,k_y,z,\omega) = \int_{-\infty}^{\infty}\int_{-\infty}^{\infty}\int_{-\infty}^{\infty} p(x,y,z,t) e^{j(k_x x + k_y y - \omega t)} dx\, dy\, dt \tag{A3}$$

This pair exists for any xy-plane with $z \geq -d$. If we insert the Fourier transform expression (A2) for $p(\mathbf{r},t)$ into the wave equation (A1) and take the Fourier transform, we obtain the following one-dimensional differential equation in z:

$$\left[\frac{\partial^2}{\partial z^2} + k_z^2\right] P(k_x,k_y,z,\omega) = 0, \quad k_z^2 \equiv k^2 - k_x^2 - k_y^2, \quad z \geq -d \tag{A4}$$

Here, $k \equiv \omega/c$ is the wave number, ω is the temporal angular frequency and (k_x,k_y) are the spatial angular frequencies. When all sources of the sound field are in the half space $z < -d$, then the complete solution to (A4) can be written as:

$$P(k_x,k_y,z,\omega) = P(k_x,k_y,0,\omega) e^{-jk_z z}, \quad z \geq -d \tag{A5}$$

where k_z is a function of the angular frequencies (k_x,k_y,ω):

$$k_z \equiv \begin{cases} \sqrt{k^2 - k_x^2 - k_y^2} & \text{for } k_x^2 + k_y^2 \leq k^2 \quad \text{(plane waves)} \\ -j\sqrt{k_x^2 + k_y^2 - k^2} & \text{for } k_x^2 + k_y^2 > k^2 \quad \text{(evanescent waves)} \end{cases} \qquad k \equiv \frac{\omega}{c} \tag{A6}$$

The circle in the spatial frequency plane which is defined by $k_x^2 + k_y^2 = k^2$ is called the radiation circle. High spatial frequencies outside the radiation circle (evanescent waves) are seen from Equations (A5) and (A6) to be exponentially attenuated in the direction away from the source.

Since the sound pressure field is measured in the plane $z = 0$, the plane wave spectrum P can be obtained from equation (A3) with $z = 0$. Equations (A5) and (A2) then allow the sound pressure field p for any $z \geq -d$ to be calculated.

Using the acoustical equation of motion, the particle velocity vector $\mathbf{u}(\mathbf{r},t)$ can be shown to be (see for example Reference 1):

$$\mathbf{u}(x,y,z,t) = \frac{1}{(2\pi)^3 \rho c}\int_{-\infty}^{\infty}\int_{-\infty}^{\infty}\int_{-\infty}^{\infty} P(k_x,k_y,z,\omega)\frac{\mathbf{k}}{k} e^{-j(k_x x + k_y y - \omega t)} dk_x dk_y d\omega \tag{A7}$$

Here, $\mathbf{k} \equiv \{k_x, k_y, k_z\}^T$ is the wave number vector and ρ is the density of the homogeneous medium.

We shall see that the formulation above can be interpreted as a method based on an expansion in plane (and evanescent) waves. Equation (A2) can be seen as an expression for the pressure distribution in three dimensions. If we insert equation (A5) in (A2), then the expression takes the form of an infinite sum (an integral) of elementary waves of the form:

$$e^{-j\mathbf{k}\cdot\mathbf{r}} = e^{-j(k_x x + k_y y + k_z z)}$$

$$p(\mathbf{r},t) = \frac{1}{(2\pi)^3}\int_{-\infty}^{\infty}\int_{-\infty}^{\infty}\int_{-\infty}^{\infty}\left[P(k_x,k_y,0,\omega)e^{j\omega t}\right] e^{-j\mathbf{k}\cdot\mathbf{r}}\, dk_x\, dk_y\, d\omega \tag{A8}$$

For spatial frequencies (k_x,k_y) inside the radiation circle, these elementary waves are plane waves propagating in the direction given by the unit vector $\hat{\mathbf{k}} \equiv \mathbf{k}/k$. The particle velocity distribution of each elementary plane wave $e^{-j\mathbf{kr}}$ is given by the vector function $(\rho c)^{-1} e^{-j\mathbf{k}\cdot\mathbf{r}}\hat{\mathbf{k}}$, ρc being the free space specific acoustic impedance. The particle velocity distribution of the total sound field can now be obtained by replacing the elementary plane wave pressure function $e^{-j\mathbf{kr}}$ in equation (A8) with the elementary particle velocity function $(\rho c)^{-1} e^{-j\mathbf{k}\cdot\mathbf{r}}\hat{\mathbf{k}}$ of the plane wave:

$$\mathbf{u}(\mathbf{r},t) = \frac{1}{(2\pi)^3 \rho c}\int_{-\infty}^{\infty}\int_{-\infty}^{\infty}\int_{-\infty}^{\infty}\left[P(k_x,k_y,0,\omega)e^{j\omega t}\right] e^{-\mathbf{k}\cdot\mathbf{r}}\hat{\mathbf{k}}\, dk_x\, dk_y\, d\omega \tag{A9}$$

This equation is equivalent to formula (A7). Equation (A9) can be obtained by insertion of Equation (A5) in (A7).